Materials Science

AIMS Materials Science, 10(4): 725–740.
DOI: 10.3934/matersci.2023040
Received: 04 July 2023
Revised: 21 July 2023
Accepted: 23 July 2023
Published: 24 August 2023

http://www.aimspress.com/journal/Materials

Research article

Influence of helium plasma on the structural state of the surface carbide layer of tungsten

Mazhyn Skakov[1,3], Arman Miniyazov[2,3,*], Victor Baklanov[2], Alexander Gradoboev[4], Timur Tulenbergenov[2,3], Igor Sokolov[2,3], Yernat Kozhakhmetov[2], Gainiya Zhanbolatova[2] and Ivan Kukushkin[2]

[1] National Nuclear Center of the Republic of Kazakhstan, Kurchatov, Kazakhstan
[2] "Institute of Atomic Energy" Branch RSE NNC RK, Kurchatov, Kazakhstan
[3] Shakarim University, Semey, Kazakhstan
[4] National Research Tomsk Polytechnic University, Tomsk, Russia

* **Correspondence:** Email: miniyazov@nnc.kz; Tel: +7-701-310-0707.

Abstract: This paper presents the results of the experimental studies of the helium plasma interaction with a surface carbide layer of tungsten. The experiments were carried out on a plasma beam installation (PBI) at a constant energy of incoming ions of 2 keV and at a surface temperature of the tungsten carbide layer of ~905 and ~1750 °C. The local parameters (T_e, n_0) of the helium plasma were evaluated using the probe method and spectrometric analysis of the plasma composition. The helium plasma irradiated two types of the carbide layer on the tungsten surface, WC and W_2C. The mechanisms of changing the tungsten surface morphology in the result of the plasma irradiation have been described. The study of the surface structure of the tungsten samples with a carbide layer of two types (WC, W_2C) after the exposure to the helium plasma has revealed two different types of the formation of helium bubbles and changes in the surface morphology. The physical mechanism of the formation of helium bubbles consists in the capture of helium atoms by the thermal vacancies generated at high temperature by the material surface. However, with a significant increase in temperature to 1750 °C, the formation of the bubbles was no longer observed and the sample surface had a developed coral-like structure with crystallographically oriented grains.

Keywords: tungsten; tungsten carbide layer; simulation experiments; helium plasma; plasma beam installation; structural state of tungsten

1. Introduction

As is known, the surfaces of the plasma-facing components (PFC) are exposed to high temperatures and fluxes of high-energy particles in thermonuclear reactors, both in stationary operating modes of the tokamaks and in non-stationary peripheral plasma instabilities and plasma disruptions [1]. Moreover, the changes in the macrostructure, recrystallization, erosion, melting, cracking and re-deposition of the particles as well as the formation of the inhomogeneous and porous layers are observed on the tungsten surface under the plasma-thermal loading [2–4]. In accordance with the expected conditions in the ITER divertor region, the tungsten will be exposed to the helium ions with an energy from 10^1 to 10^4 eV and a flux of $\geq 10^{22}$ ion/m^2·s [2,3]. It has become known that when exposed to the helium plasma, fuzz, a layer of microscopic elements with a high content of voids on the surface, is formed on the tungsten surface and the formation of helium blisters has been also established [5–13]. The formation of the blisters is significantly influenced by the ion beam parameters (ion fluence, to a lesser extent its energy, flux density, angle of the incidence), the properties of a solid body (elemental composition, temperature, structure, pretreatment) and the conditions of their interaction (solubility, diffusion coefficient, chemical reactions) [7,8].

In [14–23], the processes of blister formation and flecking under the influence of the helium plasma were experimentally studied on the linear plasma installations PISCES, NAGDIS-II, etc. It has been established that the degree of the layer porosity and depth depend on the intensity of the flux of the bombarding helium ions and their fluence.

It is also known that many thermonuclear installations use tungsten coatings applied to graphite, carbon-graphite materials or graphite materials without coating, for example, at Kazakhstan Materials Science Tokamak (KTM) [24]. Mixed layers of carbides will be formed on the tungsten plasma-facing surfaces in the result of the erosion of the graphite materials in the operating chamber of the thermonuclear installations [25,26]. At the same time, as the analysis of the literature shows, the influence of the carbide phases on the evolution of the tungsten surface morphology during the interaction with high-temperature plasma has not been fully studied. The authors of [27] studied the effect of the carbon impurity in a beam of ions bombarding the tungsten surface made by powder metallurgy. The experiments were carried out at a target temperature of 653 K. In the work, the blisters were found in the tungsten surface layers when they were irradiated with hydrogen ions.

At the same time, the plasma beam installations have proven themselves for studying the basic process regularities that occur under the action of plasma on a solid body surface. Although the existing simulation installations can reproduce only individual damaging factors of a thermonuclear reactor, they have proved to be very effective in conducting the experimental studies of candidate materials of the thermonuclear reactor [28–37]. Thus, an experimental simulation bench with a plasma-beam installation was designed on the basis of branch "Institute of Atomic Energy" of the National Nuclear Center of the Republic of Kazakhstan to test the samples of the promising structural materials and to set up the diagnostic equipment for the thermonuclear reactors [38]. The installation allows testing the candidate materials under the conditions of complex exposure to the plasma flux and a powerful thermal load. It should be noted that the temperature and density of the generated plasma are close to the parameters of the scrap-off layer (SOL) plasma in modern plasma installations [39,40]. SOL absorbs most of the plasma ejection (particles and heat) and transfers it along the force lines to the plates of the thermonuclear reactor divertor. Consequently, this area is of a paramount importance in the design of future thermonuclear reactors and the ongoing research [41,42] confirms the relevance

and practical importance of the studying processes that directly influence the plasma-converted surfaces of the thermonuclear reactor materials.

In connection with the above, the goal of this work is an experimental study of the influence of the carbide layer on the processes of the helium plasma interaction with the tungsten surface.

2. Materials and methods

The experiments were carried out on a plasma-beam installation using advanced high-precision methods for analyzing the plasma composition (optical and mass spectrometry) and monitoring the experiment conditions (temperature control, pressure, etc.). The PBI allows conducting the study of simulating the influence of the plasma and electron beam on the materials under operating conditions of the thermonuclear installations. The installation is also aimed at checking calculation models and testing the measuring and diagnostic techniques for determining the plasma parameters.

To implement the irradiation of the helium plasma, the tungsten samples in the initial state (1-W, 2-W) and the samples with a carbide layer (3-WC, 4-WC, 5-W_2C, 6-W_2C) were used.

The nature of the changes in the tested samples after the carbidization was determined by visual inspection from a macro photograph of the surface. The images of the surface of the studied samples were obtained using a Canon EOS 1200D camera.

The work on the quantitative and qualitative assessment of the microstructure of the samples was carried out on an optical microscope (TIM 5) using the software AXALIT for analyzing the microstructure [43]. Before starting the work, the value of each pixel in the image was calculated using an OM-O type object micrometer (the length of the main scale is 1.0 mm, the limits of the permissible absolute measurement error are ±0.001 mm).

The microstructure and elemental composition of the samples were studied in the topographic and compositional contrast mode using a TescanVega3 scanning electron microscope with an X-Act energy dispersion spectral analysis prefix.

The X-ray phase analysis of the samples was performed on an Empyrean diffractometer in a scanning linear detector operation mode. The exposure time (time per step) during the shooting was 30.6 seconds, the scanning step size for diffractograms was 0.026°2θ and the studied angular range was 5 ÷ 153º2θ. Radiation was Cu-Kα, voltage was 45 kV and current was 40 mA. A fixed divergence slit with an angular divergence of 1°, an anti-scattering slit of 2° and an incident beam mask with a marking of 20, providing a width of the incident beam of 19.9 mm were used. Diffractograms were processed using HighScore specialized software. The contact method was used to evaluate the changes in the surface roughness of the samples after the helium plasma irradiation using Mitutoyo Surftest SJ-410 profilometer.

In this work, the mode of beam-plasma influence on tungsten was used [38]. The vacuum system of the PBI provided a pressure of $<10^{-6}$ Torr, as it was evidenced by the mass spectrum of the residual gas in the interaction chamber in Figure 1, recorded using CIS-100 quadrupole mass spectrometer.

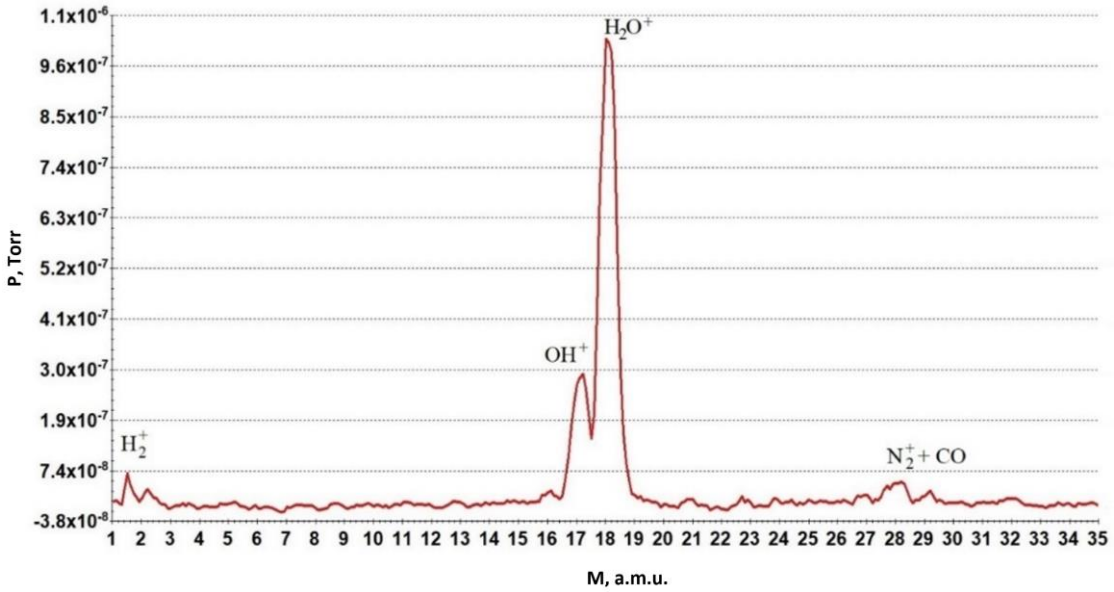

Figure 1. Mass spectrum of the residual gas in the interaction chamber.

The analysis of the mass spectrum with a range of the analyzed masses from 1 to 35 has shown that the maximum peaks fell on mass numbers 17 and 18 (water vapor). Peaks corresponding to mass numbers 2 (H_2^+) and 28 ($N_2^+ + CO$) were also observed. A high peak of the water vapor is a characteristic predominant residual gas after the exposure to the air atmosphere as a result of physical desorption from the oxidized surfaces of the inner walls of the chambers [44].

The initial tungsten samples were the discs cut out of the high purity grade rod by the electro-erosion method with a height of 2.0 ± 0.1 mm and a diameter of 10.0 ± 0.1 mm (S ~0.78 cm^2). Before the irradiation with the helium ions, all samples were subjected to recrystallization annealing on the PBI in the direct heating mode followed by a carbide layer formation. The recrystallization annealing was used to eliminate the cold work caused by the plastic deformation, which occurred during the manufacture (dragging) of the rods. The annealing of the samples was carried out using the software control of the electron beam power at a heating rate of 50 °C/min. The temperature of the samples during the annealing was 1350 ± 10 °C for 60 minutes. The temperature control on the irradiated surface was carried out by a non-contact method using ISR6 two-wave pyrometer. On the back side, the temperature was measured by the contact method using a WR-5/20 type tungsten-rhenium thermocouple. The results are presented in more detail in work [45].

Obtaining of a carbide layer (WC, W_2C) on the surface of the tungsten samples was carried out in accordance with the method previously developed by us [46–48]. The results of the studies of the carbidization process and identification of the tungsten surface layer are described in [49–51].

3. Results and discussion

As a result, the samples shown in Figure 2 were prepared for studying the interaction of the helium plasma with the tungsten carbides.

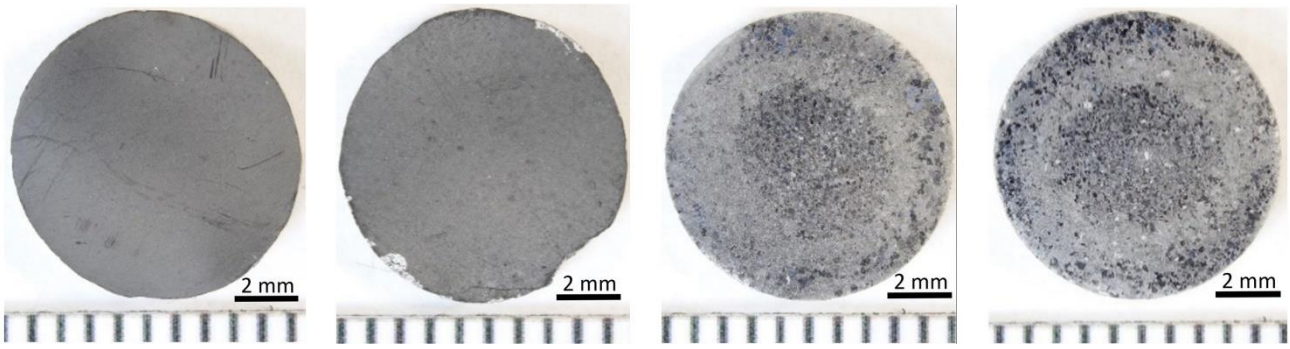

(a) WC-3 (b) WC-4 (c) W_2C-5 (d) W_2C-6

Figure 2. Appearance of tungsten samples after carbidization experiments.

After the carbidization, the surface of the samples, regardless of the experimental conditions, is characterized by the metallic luster absence, unlike the initial samples. The surface of WC-3 and WC-4 samples are characterized by the presence of a dark shade layer, while they have visually detectable brushed zones. No other visible defects have been found on the surface of the samples, with the exception of sample WC-4 where large chips have been observed at the edges, which were formed as a result of fixing the sample into the target unit of the plasma beam installation. When examining samples W_2C-5 and W_2C-6, an intermediate area with a brushed light gray shade is observed on the surface. At the same time, a grain structure with a diameter of about Ø4.5 mm is observed in the central section passing into an intermediate section with the brushed area, with a width of about 1 mm (inner ~Ø4.5 mm, outer ~Ø5.5 mm). Closer to the circumference, there is a transition back to a structure similar to the central section with a slight enlargement of the grain structure. Those were the tungsten samples that were the object of the study in this work.

The samples fixed on the target unit in the interaction chamber of the PBI were exposed to the helium plasma. To generate the plasma, an electron beam was formed and helium was supplied through the working gas intake system up to a pressure of $(1.0 \div 1.2) \times 10^{-3}$ Torr in the interaction chamber. The evaluation of the plasma parameters depending on the irradiation modes was carried out using the classical methods of the contact probe diagnostics [52].

The processing of the current voltage characteristic obtained using the proprietary plasma diagnostics system and the calculation of the local parameters were carried out by the standard methods [52] using QtiPlot software for the analysis and visualization of the research data. The data was recorded in the real time mode. Table 1 shows the results of the evaluation of the plasma parameters.

Table 1. Parameters of the experiments on the influence of helium plasma on tungsten.

Samples	W surface temperature (T_{surf}), °C	Plasma concentration (n_0), m^{-3}	Electron temperature (T_e), eV	Ion flux, $m^{-2}s^{-1}$	Ion fluence, m^{-2}
1 (W), 3 (WC), 5 (W_2C)	905	2.78×10^{18}	7.39	7.65×10^{21}	8.26×10^{25}
2 (W), 4 (WC), 6 (W_2C)	1750	2.52×10^{18}	7.69	1.10×10^{21}	7.48×10^{25}

The irradiation temperatures were determined based on the results of the previously carried out computational modeling of the thermal load on a plasma-turned tungsten monoblock of a divertor with a carbide layer under the ITER operating conditions [53]. According to the results of the computational modeling, the temperature of 905 °C corresponds to a thermal load of ~10 MW/m^2 and 1750 °C corresponds to 20 MW/m^2.

To estimate the ion current density on the sample, an aperture diaphragm with a hole of Ø10 mm was installed, shown in Figure 3, the beam diameter was about 10 mm respectively. The ion current density was ~0.8 mA/mm^2.

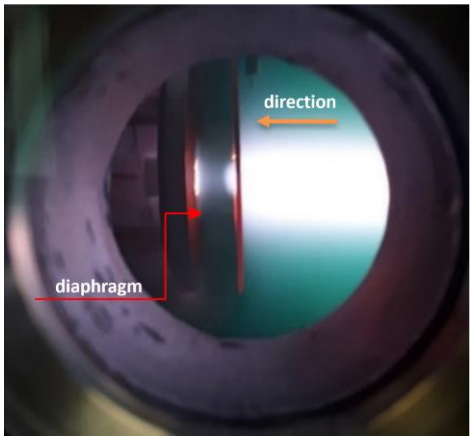

Figure 3. Location of aperture diaphragm in the interaction chamber in the process of tungsten irradiation with helium plasma.

Figures 4 and 5 show the macro images of the surface of the tungsten samples without a carbide layer and with the presence of carbides after the irradiation with the helium plasma. Samples W-1, WC-3 and W$_2$C-5 irradiated with the helium plasma at a temperature of ~905 °C are characterized by a light gray brushed shade with the presence of local areas with a grain structure. This structure has a clear outline in the form of a ring with a width of 1.5 mm (inner Ø = 5.5 mm and outer Ø = 7 mm) for W-1 sample, without a carbide layer.

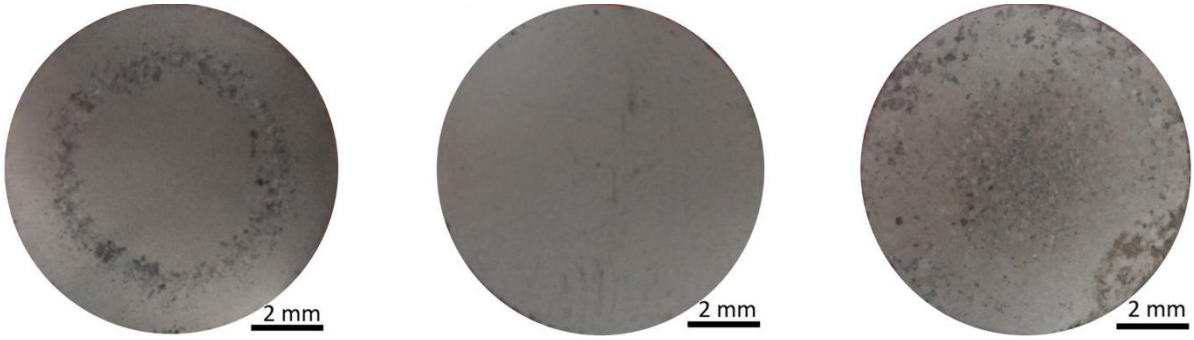

Tungsten without a carbide layer W-1 | Tungsten with a carbide layer WC-3 | Tungsten with a carbide layer W$_2$C-5

Figure 4. Appearance of the surface of tungsten samples irradiated with helium plasma at ~905 °C.

The surfaces of samples W-2, WC-4 and W_2C-6 irradiated at ~1750 °C are characterized by a continuous grain structure, while the presence of large grains is observed on the circumference of the surface of samples W-2 and W_2C-6 (Figure 5). WC-4 sample has a uniform fine-grained structure.

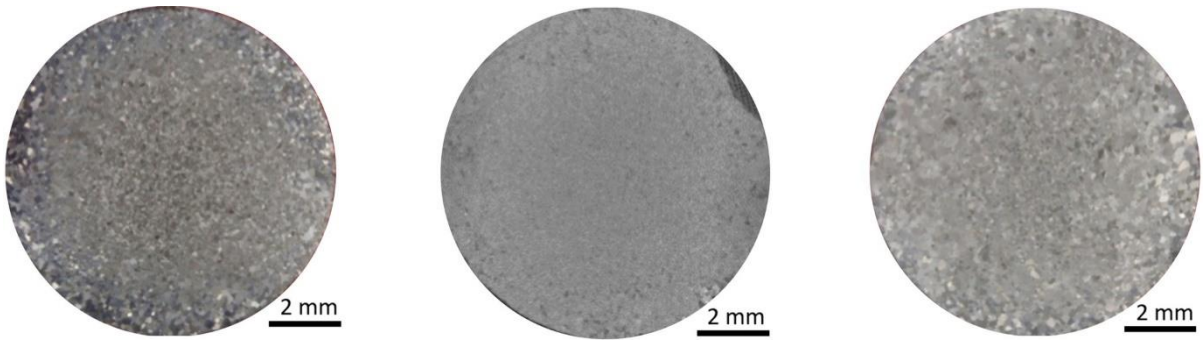

Tungsten without a carbide layer W-2 | Tungsten with a carbide layer WC-4 | Tungsten with a carbide layer W_2C-6

Figure 5. Appearance of the surface of tungsten samples irradiated with helium plasma at ~1750 °C.

Figure 6 shows SEM-images of the surface structure of the initial tungsten samples after the exposure to the helium plasma. The tungsten surface irradiated at a temperature of ~905 °C is characterized by the formation of randomly arranged helium bubbles of micron and submicron sizes (Figure 6a). In the high-temperature irradiation mode, the main role in the growth of the bubbles is played by their coalescence as a result of the thermal migration process and the high irradiation temperature resulted in the formation of the bubbles up to 10 μm in size. At the same time, the bubbles were preserved in the sample surface layer due to very high binding energy with the helium. It is assumed that the physical mechanism of forming the helium bubbles consists in the capture of the helium atoms by the thermal vacancies generated at the high temperature of the material surface.

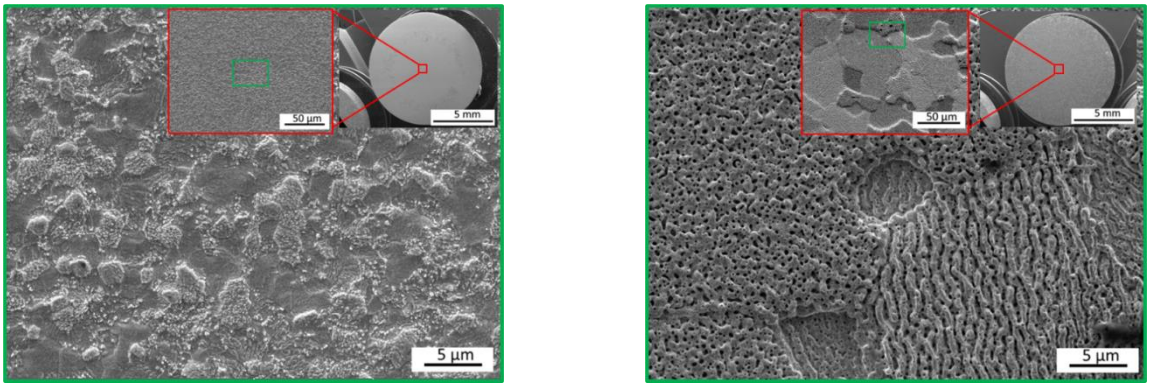

(a) W-1 (~905 °C) (b) W-2 (~1750 °C)

Figure 6. Microstructure of tungsten without a carbide layer after the exposure to helium plasma.

However, this type of the bubble formation was not observed at high irradiation temperature ~1750 ℃ (Figure 6b). Figure 6b shows that the sample surface has a developed coral-like surface, with the presence of a certain orientation within each grain. As it is known [54], the resistance of the tungsten surface to various types of exposure directly depends on the orientation of each individual grain. It can be assumed that the change in the morphology of the tungsten surface has a grain-oriented character. Accordingly, such changes in the sample surface are a consequence of the morphology evolution, which was observed on the sample irradiated at ~905 °C. This is due to the formation of the helium bubbles, the upper part of which collapses, forming voids or holes which diameter reaches 9.5 ± 2.3 nm. The migration of the helium bubbles causes pitting of the surface to a surface density of about 875 ± 30 pits/μm^{-2} [55], after which the statistical changes in the number and location of the formed voids begin to create pimples and dimples.

Figure 7 shows SEM-images of the surface structure of the tungsten samples with two types of the carbide layers (WC and W_2C) irradiated at temperatures of ~905 and ~1750 °C. The analysis of the results has shown that the microstructure of the samples (Figure 7a,b) is characterized by a developed morphology similar to the sample without a carbide layer, which was irradiated at ~1750 °C. However, in the case of the samples with a carbide layer, the sizes of the holes on the surface with the formation of the pimples and dimples are significantly smaller. At the same time, the sample surface with a carbide layer irradiated at ~905 °C has a similar character as WC-2 sample, where the grain structure is still observed. The surface of sample WC-4, as can be seen from Figure 7b, has completely lost its characteristic grain structure, that is, an increase in temperature has resulted in a complete overcoming of the orientation dependence of the grains.

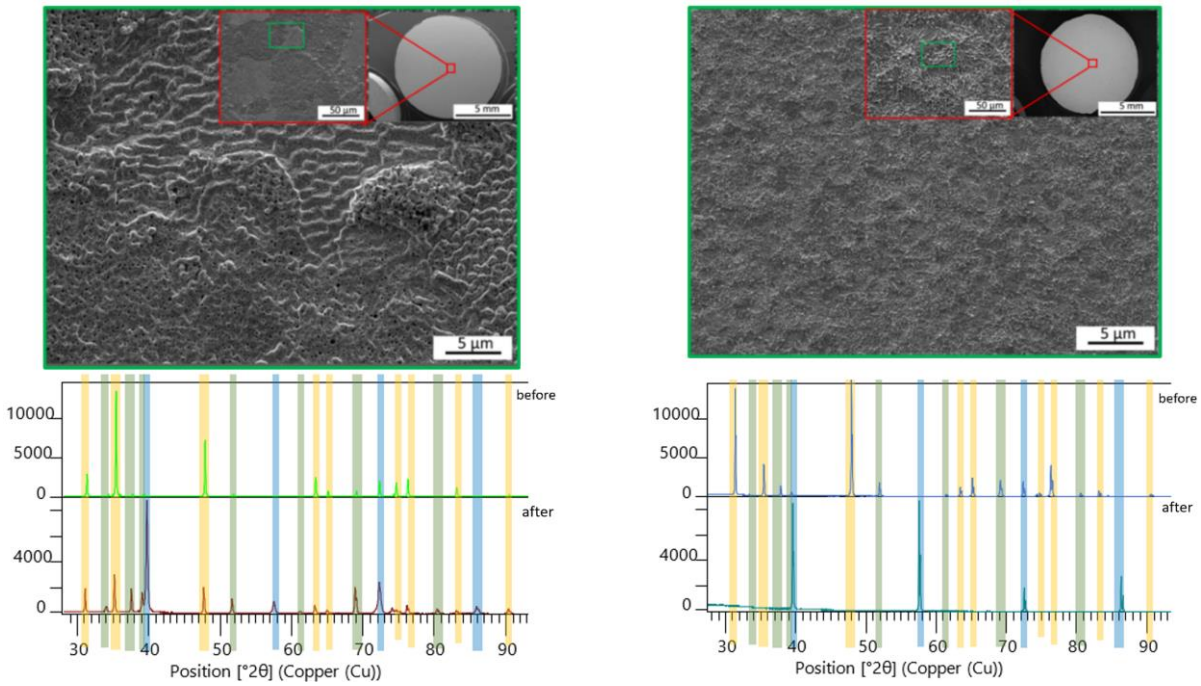

(a) WC-3 (~905 °C) (b) WC-4 (~1750 °C)

Figure 7. Microstructure and phase composition of the tungsten surface with a WC-based carbide layer after the exposure to helium plasma (yellow color indicates the localization of the peaks of the WC phase, green—the W_2C phase, blue—the peaks of W).

In the case of the samples with a carbide layer of tungsten semi-carbide (Figure 8a,b), a similar picture is seen with W-1 sample (Figure 6a), but without the formation of the micron helium bubbles, which indicates a high resistance to the bubble coalescence and restriction of their migration. It is clear that the migration and coalescence of the helium bubbles play an essential role in the formation of such peculiar structure. However, in the case of W_2C-6 sample, a high concentration and uniform distribution of helium bubbles is observed, whereas such bubbles are randomly located in smaller numbers on the surface of W_2C-5 sample.

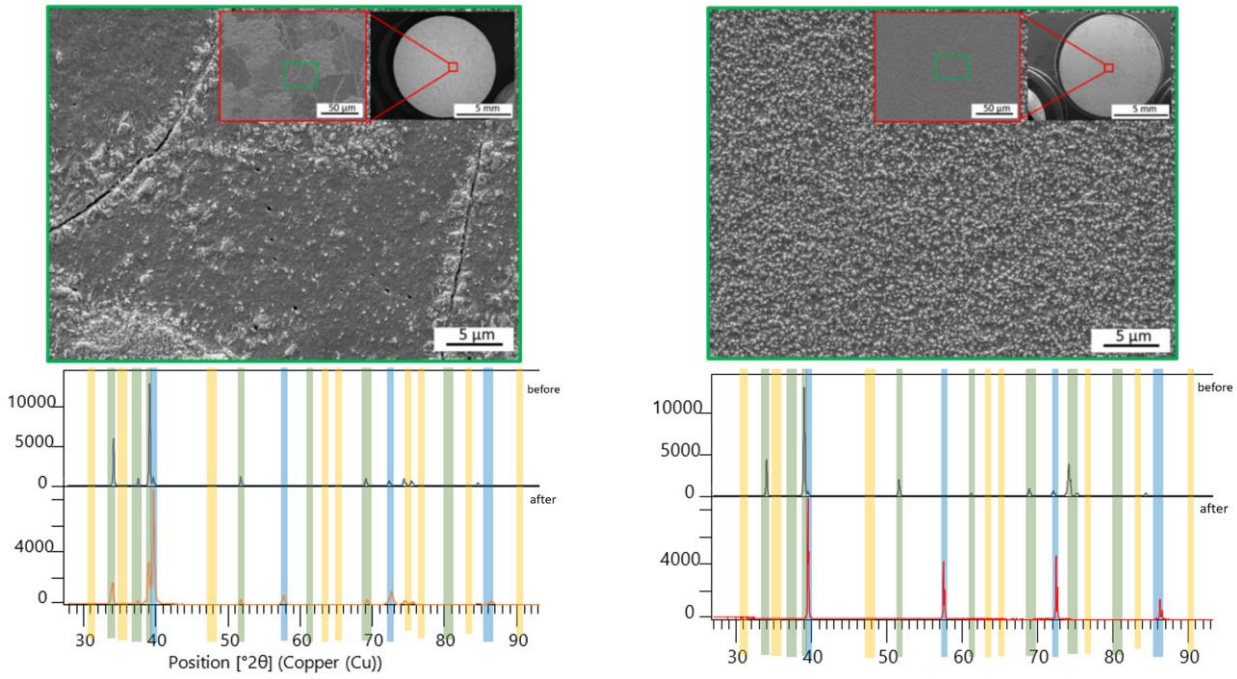

(a) W_2C-5 (~905 °C) (b) W_2C-6 (~1750 °C)

Figure 8. Microstructure and phase composition of the tungsten surface with a W_2C-based carbide layer after the exposure to helium plasma (yellow color indicates the localization of the peaks of the WC phase, green—the W_2C phase, blue—the peaks of W).

The impact of helium plasma on tungsten with a carbide layer at a temperature of 905 °C led to partial sputtering of the carbide layers, as evidenced by a decrease in the peaks WC, W_2C and the appearance of peaks W. After the impact of helium plasma at a temperature of 1750 °C, only peaks belonging to W are observed. This can be explained by the difficulty of identifying the type of carbide phases, since diffraction patterns carry information about the structural state of the material with a thickness of ~1.6 µm (at an angle of $2\theta \sim 40°$) to ~4.2 µm (at an angle of $2\theta \sim 90°$). This indicates that the thickness of the carbide layer does not exceed 4 µm and that it is sputtered at a high irradiation temperature.

The microstructure of the surface of the samples with a W_2C-based carbide layer after the exposure to the helium plasma at different temperatures have a similar morphology. The results of the analysis of the grain sizes and their quantity after the plasma irradiation are shown in Figure 9 in the form of histograms of the distribution of conditional grain sizes in points. According to standard ASTM

E112-13 [43], a smaller value of the grain number corresponds to a larger grain size, and a larger value corresponds to a smaller grain size (Table 2). A comparative analysis with a sample of the initial tungsten has shown that the samples with a W_2C-based carbide layer are characterized by a slight decrease in the grain sizes. At the same time, a large number of crack networks are observed on the surface of all samples with a carbide layer exposed at ~905 °C.

Table 2. Grain size relationships computed for uniform, randomly oriented, equiaxed grains [43].

Grain Size No.	Average Diameter
0	359.2
…	…
4.5	75.5
5	63.5
5.5	53.4
6	44.9
6.5	37.8
7	31.8
7.5	26.7
8	22.5
8.5	18.9
9	15.9
9.5	13.3
10	11.2
10.5	9.4
11	7.9
11.5	6.7
12	5.6
12.5	4.7
13	4
13.5	3.3
14	2.8

According to the authors of work [56], the temperature of the tungsten thin layer increases at high thermal influences, which results in its thermal expansion and the appearance of compressive stresses in the surface layer. In this case, the material is deformed and when the temperature of the brittle-viscous transition is exceeded, a part of it becomes plastic, which leads to an increase in the surface roughness. In our case, the carbide layer has a lower thermal conductivity than the tungsten bulk. A significant temperature gradient arising between the carbide layer and the main tungsten base during its forced cooling results in the appearance of compressive stresses in the carbide layer. With the achievement of the transition temperature of brittleness to plasticity, an increase in the surface roughness of the samples is observed along with the predominance of the plastic deformation. During the cooling process, when the temperature becomes the same throughout the entire sample, tensile stresses arise. If these residual stresses exceed the tungsten strength threshold, its surface cracks. When a network of cracks appears, the stresses are released along the surface near the cracks. This

phenomenon is particularly characteristic for the W_2C-5 sample, where a high concentration of crack networks is observed.

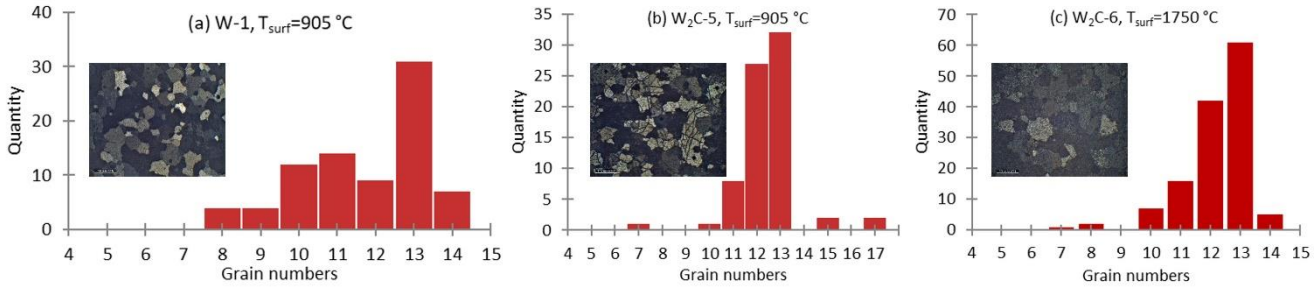

Figure 9. Microstructures and histograms of the number of grains for each grain number after plasma irradiation.

The roughness measurement was carried out on the irradiated surface from the edge to the diametrically opposite side. Figure 10 shows the comparative results of measuring the surface roughness of the tungsten samples after the irradiation with the helium plasma. These results are in good agreement with the results of the microstructural studies described above.

The analysis of the results has shown that the roughness values vary greatly depending on the carbide layer type. Plasma irradiation at a temperature of ~1750 °C leads to a higher modification of the surface relief of the samples. At the same time, the developed surface morphology is characteristic of all samples and only slightly differs depending on the initial one. The samples with a WC carbide layer, in which a significant modification of the surface is detected, are characterized by a smoother surface. Thus, according to Figure 10, at an irradiation temperature of 905 °C, the carbide layer can act as a protective barrier layer during helium plasma irradiation, but an increase in temperature obviously leads to the destruction of the barrier layer.

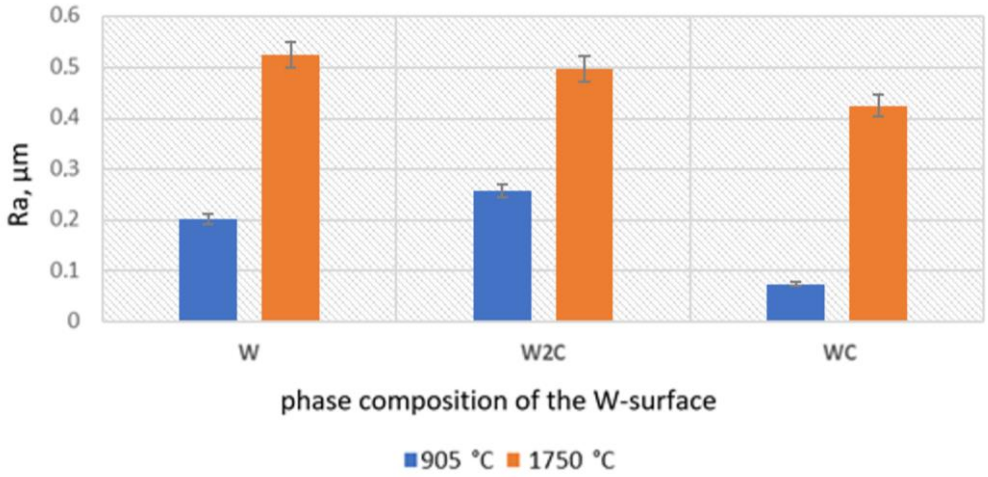

Figure 10. Surface roughness of tungsten samples after the irradiation with helium plasma depending on the irradiation modes and carbide layer type.

4. Conclusions

Thus, the following conclusions can be drawn from the analysis of the experimental data obtained on the interaction of the helium plasma with the tungsten surface with a carbide layer:

• The dependence of the change in tungsten roughness on the carbide layer and the irradiation temperatures has been established. A noticeable modification of the surface of the samples is observed at high irradiation temperature.

• The topography of the surface of the tungsten samples after irradiation at different temperatures indicates a significant influence of temperature on the surface structure and morphology. The samples with a carbide layer have comparatively smaller holes and pimples than the initial tungsten surface.

• Comparatively low heat conductivity of the surface carbide layer relative to the tungsten base has led to the appearance of the compressive stresses in the carbide layer. When the temperature of the brittleness transition to plasticity is reached, an increase in the surface roughness of the samples is observed along with the plastic deformation predominance. In the process of tungsten cooling, the tensile stresses arise which can lead to surface cracking if the tungsten strength limit is exceeded. The appearance of the crack network of the surface of the samples, especially on W_2C-5 sample, is associated with the release of stresses along the surface close to the cracks.

• It has been noted that on the surface of the tungsten samples with a carbide layer, a similar morphology with the initial tungsten surface as the irradiation result is observed. However, there are significantly smaller holes sizes on the surface. There is a loss of the grain structure and a complete overcoming of the orientation dependence of the grains with the temperature increase. In the case of the samples with the tungsten semi-carbide, the migration and coalescence of helium bubbles play a significant role in the structure formation.

• It has been established that helium bubbles form in the carbide layer when exposed to plasma at low temperatures. This is due to the fact that at a low irradiation temperature, no significant destruction of the carbide layer occurs. Therefore, when exposed to helium plasma, the formation of bubbles is mainly localized in the carbide layer. The detection of helium bubbles in the tungsten itself indicates the destruction of the carbide layer and thus their formation occurs in the tungsten bulk at a high temperature of plasma irradiation.

In conclusion, it should be noted that the study of carbide layer influence on the interaction of helium plasma with tungsten revealed two types of helium bubble formation and changes in the surface morphology. The physical mechanism of forming helium bubbles consists of the capture of helium atoms by the thermal vacancies generated at high material surface temperature. However, at a high irradiation temperature of 1750 °C, the formation of bubbles was not observed and the surface of the sample had a developed coral-like structure with crystallographically oriented grains. This indicates the surface morphology evolution is caused by the formation of helium bubbles, the upper part of which collapses, forming voids or holes. In the result of the study's implementation, new data about the processes occurring on the tungsten surface with a carbide layer when exposed to the helium plasma has been obtained.

Use of AI tools declaration

The authors declare they have not used Artificial Intelligence (AI) tools in the creation of this article.

Acknowledgments

This research was conducted within the framework of Program No. BR09158585 "Scientific and technical support of experimental studies at the Kazakhstani Material Testing Tokamak KTM".

Conflict of interest

The authors declare no conflict of interest.

References

1. Pintsuk G, Hasegawa A (2020) Tungsten as a plasma-facing material, In: Konings RJM, Stoller RE, *Comprehensive Nuclear Material*, 2 Eds., Oxford: Elsevier.
2. Rieth M, Doerner R, Hasegawa A, et al. (2019) Behavior of tungsten under irradiation and plasma interaction. *J Nucl Mater* 519: 334–368. https://doi.org/10.1016/j.jnucmat.2019.03.035
3. Bolt H, Barabash V, Federici G, et al. (2002) Plasma facing and high heat flux materials-needs for ITER and beyond. *J Nucl Mater* 307–311: 43–52. https://doi.org/10.1016/S0022-3115(02)01175-3
4. Suchandrima D (2019) Recent advances in characterising irradiation damage in tungsten for fusion power. *SN App Sci* 1: 1614. https://doi.org/10.1007/s42452-019-1591-0
5. Hammond KD (2017) Helium, hydrogen, and fuzz in plasma-facing materials. *Mater Res Express* 4: 104002. https://doi.org/10.1088/2053-1591/aa8c22
6. Henriksson K, Nordlund K, Krasheninnikov A, et al. (2017) The depths of hydrogen and helium bubbles in tungsten: A comparison. *Fusion Sci Technol* 5: 43–57. https://doi.org/10.13182/FST06-A1219
7. Tsitrone E (2022) Investigation of plasma wall interactions between tungsten plasma facing components and helium plasmas in the WEST tokamak. *Nucl Fusion* 62: 076028. https://doi.org/10.1088/1741-4326/ac2ef3
8. Kajita S, Takamura S, Ohno N (2009) Prompt ignition of a unipolar arc on helium irradiated tungsten. *Nucl Fusion* 49: 032002. https://doi.org/10.1088/0029-5515/49/3/032002
9. Valles G, Martin-Bragado I, Nordlund, K, et al. (2017) Temperature dependence of underdense nanostructure formation in tungsten under helium irradiation. *J Nucl Mater* 490: 108–114. https://doi.org/10.1016/j.jnucmat.2017.04.021
10. Skakov M, Kurbanbekov S, Baklanov V, et al. (2016) Structure investigations of siliconized graphite obtained during elaboration of sintering process technology. *Int J ChemTech Res* 9: 447–452. Available from: https://sphinxsai.com/2016/ch_vol9_no8/2/(447-452)V9N8CT.pdf.
11. Kajita S, Sakaguchi W, Ohno N, et al. (2009) Formation process of tungsten nanostructure by the exposure to helium plasma under fusion relevant plasma conditions. *Nucl Fusion* 49: 095005. https://doi.org/10.1088/0029-5515/49/9/095005.
12. Takamura S, Ohon N, Nishijima D, et al. (2006) Formation of nanostructured tungsten with arborescent shape due to helium plasma irradiation. *Plasma Fusion Res* 1: 051. https://doi.org/10.1585/pfr.1.051
13. Tulenbergenov TR, Skakov MK, Sokolov IA, et al. (2019) Formation of "fuzz" on the pre-nitrided tungsten surface. *Phys Atom Nuclei* 82: 1454–1459. https://doi.org/10.1134/S1063778819120299

14. Ueda Y, Peng HY, Lee HT, et al. (2013) Helium effects on tungsten surface morphology and deuterium retention. *J Nucl Mater* 44: S267–S272. https://doi.org/10.1016/j.jnucmat.2012.10.023
15. Takamura S (2014) Initial stage of fiber-form nanostructure growth on refractory metal surfaces with helium plasma irradiation. *Plasma Fusion Res* 9: 1302007. https://doi.org/10.1585/pfr.9.1302007
16. Nishijima D, Ye MY, Ohno N, et al. (2003) Incident ion energy dependence of bubble formation on tungsten surface with low energy and high flux helium plasma irradiation. *J Nucl Mater* 313–316: 97–101. https://doi.org/10.1016/S0022-3115(02)01368-5
17. Nishijima D, Ye MY, Ohno N, et al. (2004) Formation mechanism of bubbles and holes on tungsten surface with low-energy and high-flux helium plasma irradiation in NAGDIS-II. *J Nucl Mater* 329–333: 1029–1033. https://doi.org/10.1016/j.jnucmat.2004.04.129
18. Takamura S, Ohno N, Nishijima D, et al. (2006) Formation of nanostructured tungsten with arborescent shape due to helium plasma irradiation. *Plasma Fusion Res* 1: 051. https://doi.org/10.1585/pfr.1.051
19. Baldwin MJ, Doerner RP (2008) Helium induced nanoscopic morphology on tungsten under fusion relevant plasma conditions. *Nucl Fusion* 48: 035001. https://doi.org/10.1088/0029-5515/48/3/035001
20. Baldwin MJ, Doerner RP (2010) Formation of helium induced nanostructure "fuzz" on various tungsten grades. *J Nucl Mater* 404: 165–173. https://doi.org/10.1016/j.jnucmat.2010.06.034
21. Temmerman GD, Bystrov K, Doerner RP, et al. (2013) Helium effects on tungsten under fusion-relevant plasma loading conditions. *J Nucl Mater* 438: S78–S83. https://doi.org/10.1016/j.jnucmat.2013.01.012
22. Wright GM, Brunner D, Baldwin MJ, et al. (2003) Tungsten nanotendril growth in the Alcator C-Mod divertor. *Nucl Fusion* 52: 042003. https://doi.org/10.1088/0029-5515/52/4/042003
23. Miyamoto M, Mikami S, Nagashima H, et al. (2015) Systematic investigation of the formation behavior of helium bubbles in tungsten. *J Nucl Mater* 463: 333–336. https://doi.org/10.1016/j.jnucmat.2014.10.098
24. Tazhibayeva IL, Azizov EA, Krylov VA, et al. (2005) KTM experimental complex project status. *Fusion Sci Technol* 47: 746–750. https://doi.org/10.13182/FST05-A77
25. Zhou HB, Ou X, Zhang Y, et al. (2013) Effect of carbon on helium trapping in tungsten: A first-principles investigation. *J Nucl Mater* 440: 338–343. https://doi.org/10.1016/j.jnucmat.2013.05.070
26. Zhanbolatova GK, Baklanov VV, Skakov MK, et al. (2021) Influence of temperature on tungsten carbide formation in a beam plasma discharge. *J Phys-Conf Ser* 2064: 012055. https://doi.org/10.1088/1742-6596/2064/1/012055
27. Ueda Y, Shimada T, Nishikawa M (2004) Impact of carbon impurities in hydrogen plasmas on tungsten blistering. *Nucl Fusion* 44: 62–67. https://doi.org/10.1088/0029-5515/44/1/007
28. Tulenbergenov TR, Sokolov IA, Miniyazov AZ, et al. (2019) Review on linear accelerators. *NNC RK Bulletin* 1: 59–67 (in Russian). https://doi.org/10.52676/1729-7885-2019-4-59-67
29. Sokolov IA, Skakov MK, Miniyazov AZ, et al. (2021) Interaction of plasma with beryllium. *J Phys-Conf Ser* 2064: 012070. https://doi.org/10.1088/1742-6596/2064/1/012070
30. Skakov M, Batyrbekov E, Sokolov I, et al. (2022) Influence of hydrogen plasma on the surface structure of beryllium. *Materials* 15: 6340. https://doi.org/10.3390/ma15186340

31. Tazhibayeva I, Ponkratov Y, Lyublinsky I, et al. (2022) Study of liquid tin-lithium alloy interaction with structural materials of fusion reactor at high temperatures. *Nucl Mater Energy* 30: 101152. https://doi.org/10.1016/j.nme.2022.101152
32. Kozhakhmetov YA, Skakov MK, Kurbanbekov SR, et al. (2021) Powder composition structurization of the Ti-25Al-25Nb (at.%) system upon mechanical activation and subsequent spark plasma sintering. *Eurasian Chem-Technol J* 23: 37–44. https://doi.org/10.18321/ectj1032
33. Sokolov IA, Skakov MK, Zuev VA, et al. (2018) Study of the interaction of plasma with beryllium that is a candidate material for the first wall of a fusion reactor. *Tech Phys* 63: 506–510. https://doi.org/10.1134/S1063784218040230
34. Skakov M, Yerbolatova G, Kantai N, et al. (2014) Investigation of the influence of electrolytic-plasma processing on structural-phase state and mechanical properties of the 40CrNiAl alloy. *Adv Mat Res* 1044–1045: 67–70. https://doi.org/10.4028/www.scientific.net/AMR.1044-1045.67
35. Kantay N, Rakhadilov B, Kurbanbekov S, et al. (2021) Influence of detonation-spraying parameters on the phase composition and tribological properties of Al_2O_3 coatings. *Coatings* 11: 793. https://doi.org/10.3390/coatings11070793
36. Ponkratov YV, Samarkhanov KK, Baklanov VV, et al. (2023) Investigation of the interaction of liquid tin-lithium alloy with austenitic stainless steel at high temperatures. *Fusion Eng Des* 191: 113560. https://doi.org/10.1016/j.fusengdes.2023.113560
37. Kenzhin EA, Kenzhina IE, Kulsartov TV, et al. (2023) Study of interaction of hydrogen isotopes with titanium beryllide ($Be_{12}Ti$). *Fusion Eng Des* 191: 113738. https://doi.org/10.1016/j.fusengdes.2023.113738
38. Tulenbergenov TR, Miniyazov AZ, Sokolov IA, et al. (2019) The role of simulation bench with plasma-beam installation in studies of plasma-surface interaction. *NNC RK Bulletin* 1: 51–58 (in Russian). https://doi.org/10.52676/1729-7885-2019-4-51-58
39. Krasheninnikov SI (2001) On scrape off layer plasma transport. *Phys Lett A* 283: 368–370. https://doi.org/10.1016/S0375-9601(01)00252-3
40. D'Ippolito DA, Myra J, Krasheninnikov S, et al. (2004) Blob transport in the tokamak scrape-off-layer. *Contrib Plasm Phys* 44: 205–216. https://doi.org/10.1002/ctpp.200410030
41. Loarte A, Lipschultz B, Kukushkin AS, et al. (2007) Chapter 4: Power and particle control. *Nucl Fusion* 47: S203. https://doi.org/10.1088/0029-5515/47/6/S04
42. Krasheninnikov S, D'Ippolito DA, Myra J, et al. (2008) Recent theoretical progress in understanding coherent structures in edge and SOL turbulence. *J Plasma Phys* 74: 679–717. https://doi.org/10.1017/S0022377807006940
43. ASTM International (2021) Standard test methods for determining average grain size. ASTM E112-13. https://doi.org/10.1520/E0112-13R21
44. Ivanov VI (2016) *Vacuum Technology: Textbook*, St. Petersburg: ITMO University (in Russian).
45. Skakov MK, Miniyazov AZ, Baklanov VV, et al. (2022) Method of high temperature annealing of metals and alloys by electron beam exposure in vacuum and gas medium. Patent No. 35911. Available from: https://gosreestr.kazpatent.kz/Invention/DownLoadFilePdf?patentId=346518&lang=ru.
46. Skakov MK, Sokolov IA, Batyrbekov EG, et al. (2020) Method for obtaining tungsten carbides in a plasma-beam discharge. Patent No. 34269. Available from: https://gosreestr.kazpatent.kz/Invention/DownLoadFilePdf?patentId=304053&lang=ru.

47. Skakov MK, Baklanov VV, Zhanbolatova GK, et al. (2023) Research of the structural-phase state of tungsten surface layer cross-section after carbidization in a beam-plasma discharge usage electron microscopy methods. *NNC RK Bulletin* 2: 89–96. https://doi.org/10.52676/1729-7885-2023-2-89-96
48. Baklanov V, Zhanbolatova G, Skakov M, et al. (2022) Study of the temperature dependence of a carbidized layer formation on the tungsten surface under plasma irradiation. *Mater Res Express* 9: 016403. https://doi.org/10.1088/2053-1591/ac4626
49. Miniyazov AZ, Skakov MK, Tulenbergenov TR, et al. (2021) Investigation of tungsten surface carbidization under plasma irradiation. *J Phys-Conf Ser* 2064: 012053. https://doi.org/10.1088/1742-6596/2064/1/012053
50. Skakov M, Miniyazov A, Batyrbekov E, et al. (2022) Influence of the carbidized tungsten surface on the processes of interaction with helium plasma. *Materials* 15: 7821. https://doi.org/10.3390/ma15217821
51. Skakov M, Baklanov V, Zhanbolatova G, et al. (2023) The effect of recrystallization annealing on the tungsten surface carbidization in a beam plasma discharge. *AIMS Mater Sci* 10: 541–555. https://doi.org/10.3934/matersci.2023030
52. Kozlov OV (1969) *Electrical Probe in Plasma*, Moscow: Atomizdat, 293 (in Russian).
53. Skakov M, Zhanbolatova GK, Miniyazov AZ, et al. (2021) Impact of high-power heat load and W surface carbidization on its structural-phase composition and properties. *Fusion Sci Technol* 77: 57–66. https://doi.org/10.1080/15361055.2020.1843885
54. Ohno N, Hirakata Y, Yamagiwa M (2013) Influence of crystal orientation on damages of tungsten exposed to helium plasma. *J Nucl Mater* 438: S879–S882. https://doi.org/10.1016/j.jnucmat.2013.01.190
55. Kajita S, Sakaguchi W, Ohno N, et al. (2009) Formation process of tungsten nanostructure by the exposure to helium plasma under fusion relevant plasma conditions. *Nucl Fusion* 49: 9. https://doi.org/10.1088/0029-5515/49/9/095005
56. Cherepanov D, Arakcheev A, Arakcheev A, et al. (2021) In situ method for studying stresses in a pulse-heated tungsten plate based on measurements of surface curvature. *Nucl Mater Energy* 26: 100919. https://doi.org/10.1016/j.nme.2021.100919.

AIMS Press